


## Anomalous Gilbert damping induced by the coexisting static and dynamic coupling in Fe/Pd/Fe trilayers

Yan Li,<sup>1,2</sup> Yang Li,<sup>1,2</sup> Rui Sun,<sup>1,2</sup> Na Li,<sup>1,2</sup> Zi-Zhao Gong,<sup>1,2</sup> Xu Yang ,<sup>1,2</sup> Zong-Kai Xie,<sup>1,2</sup> Hao-Liang Liu,<sup>1</sup> Wei He,<sup>1</sup> Xiang-Qun Zhang,<sup>1</sup> and Zhao-Hua Cheng<sup>1,2,3,\*</sup>

<sup>1</sup>State Key Laboratory of Magnetism and Beijing National Laboratory for Condensed Matter Physics, Institute of Physics, Chinese Academy of Sciences, Beijing 100190, China

<sup>2</sup>School of Physical Sciences, University of Chinese Academy of Sciences, Beijing 100049, China

<sup>3</sup>Songshan Lake Materials Laboratory, Dongguan, Guangdong 523808, China



(Received 29 June 2021; revised 12 August 2021; accepted 25 August 2021; published 7 September 2021)

Although the magnetic relaxation mechanism in ferromagnetic/nonmagnetic (FM/NM) bilayers has been commendably established, the nonlocal Gilbert damping has been much less addressed in spin valve configurations of FM/NM/FM associated with both the static interlayer exchange coupling and the dynamic coupling. Here, we report the dimensional crossover role of the Pd layer on magnetic relaxation in Fe/Pd/Fe trilayer structures. We identify a pronounced jump of Gilbert damping across the characteristic static interlayer exchange coupling length of Fe/Pd/Fe. The significant enhancement and suppression of Gilbert damping values are ascribed to the entanglement of the dynamics of the two Fe layers mediated by the static exchange coupling and the dynamic exchange coupling. Our work deepens the understanding to manipulate the spin transport and magnetic relaxation via the coherence of spin current.

DOI: [10.1103/PhysRevB.104.094409](https://doi.org/10.1103/PhysRevB.104.094409)

### I. INTRODUCTION

The Gilbert damping determining the magnon lifetime, the speed of the magnetic switching, and the threshold current in spin-torque devices inspires intense research interest in fundamental magnetic relaxation mechanism [1–3]. Generally, the local Gilbert damping in ferromagnetic metals is interpreted by the dissipation of energy and angular momentum from the localized  $d$  electrons mediated by the itinerant  $s$  electrons, as exemplified by the breathing Fermi surface model, the scattering theory, and the linear response model [4–6]. According to the spin pumping effect in ferromagnet (FM)/normal metal (NM) heterostructures, the nonlocal Gilbert damping arises from the spin torques related to the reflection and absorption of spin current across the FM/NM interface, which is increasingly important with the rapid progress in spintronics [7–9].

Remarkably, spin/magnon valve structures FM/NM/FM, in which the information transmission and computing can be encoded and mediated by the pure spin current with lower power dissipation rather than by charge current in conventional electronic devices, show intriguing characteristics associated with the spin current and spin transfer torque in spintronic devices [10–12]. The interlayer exchange interaction in FM/NM/FM structures entangles the dynamics of the two FM layers, and trigger collective spin excitations accompanying with the transmission of spin current [13–15]. Such a FM/NM/FM structure with the interlayer exchange interaction can be regarded as one of hybrid quantum systems exploiting quantum magnon information processing [16–18]. It is

noteworthy that the magnon or quasiparticles lifetime in such a versatile structure heavily relies on the system's damping, whereas the dissipation of spin current is strongly affected by the static interlayer exchange coupling and the dynamic exchange coupling (i.e., spin current-induced spin torque) between two FM layers [19–23]. For instance, it was stated that the coherent spin pumping can increase or suppress the nonlocal damping in the coupling yttrium iron garnet/permalloy heterostructure [18]. Subsequently, an emerging question is how to distinguish the entanglement and role of the two couplings on magnetic relaxation in FM/NM/FM multilayers. In this work, we concentrate on the nonlocal Gilbert damping in the Fe/Pd/Fe trilayers. Instead of the commonly used normal metal Pt or Cu, we use Pd hosting the static interlayer exchange coupling length  $\sim 2$  nm and the spin diffusion length  $\sim 7$  nm [23–28], in which the damping contributions from the static exchange coupling and the dynamic coupling could be easily disentangled via tuning the Pd thickness. Herein, we observed a drastic steplike Gilbert damping feature nearby the static interlayer exchange coupling length. The underlying physical mechanism is carefully addressed by separated and mutual precession modes.

### II. EXPERIMENTS

Fe (top, 7.5 nm)/Pd( $t_{\text{Pd}}$ )/Fe (bottom, 6 nm) trilayers and Pd( $t_{\text{Pd}}$ )/Fe(6 nm) bilayers ( $t_{\text{Pd}}$  indicates thicknesses in nanometer) were prepared on MgO(001) substrates by molecular beam epitaxy (MBE) with a base pressure of  $3 \times 10^{-10}$  mbar, where  $t_{\text{Pd}} = 1, 3, 5, 7, 9,$  and  $11$  nm. The MgO substrates were annealed at 700 °C for 2 h in a vacuum chamber, and then held at room temperature during deposition. All

\*Corresponding author: zhcheng@iphy.ac.cn

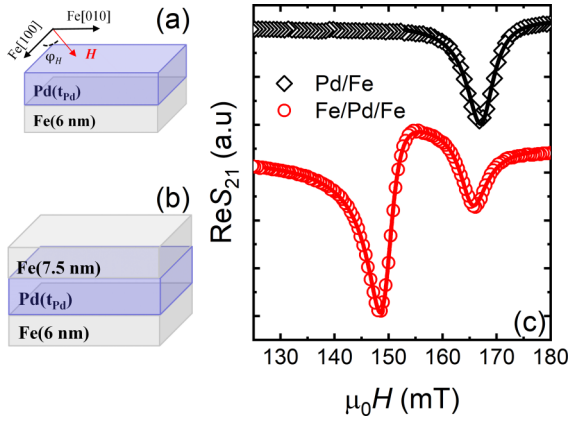


FIG. 1. Illustrations of the stacked bilayers Pd/Fe (a) and trilayers Fe/Pd/Fe (b). Real part of  $S_{21}$  vs magnetic field at 14 GHz for Pd(7 nm)/Fe(6 nm) and Fe(7.5 nm)/Pd(7 nm)/Fe (c) at ferromagnetic resonance.

Fe/Pd/Fe films were also covered by a Cu layer (3.5 nm) to avoid oxidation. The simplified schematic diagrams of the sample structures are shown in Figs. 1(a) and 1(b). The dynamic properties are measured by a broadband vector network analyzer ferromagnetic resonance (VNA-FMR) setup involving a coplanar waveguide for microwave excitation. During the measurement, the frequency and input power (0 dBm) of the microwave source were fixed while the external magnetic field was swept. The transmission

coefficients ( $S_{21}$ ) were recorded as a function of the in-plane applied magnetic field  $H$ . The sample preparation and VNA-FMR measurement were similar to our previous experiments [29–31].

### III. RESULTS AND DISCUSSION

Figure 1(c) shows the typical FMR spectra signed by the transmission coefficient  $S_{21}$  for the Pd(7 nm)/Fe(6 nm) bilayers and Fe(7.5 nm)/Pd(7 nm)/Fe(6 nm) trilayers. The corresponding resonant field  $H_r$  and linewidth  $\Delta H$  can be well fitted by using the following expression:

$$\text{Re}S_{21}(H) = S_0 + L \frac{(\Delta H/2)^2}{(H - H_r)^2 + (\Delta H/2)^2} - D \frac{(\Delta H/2)(H - H_r)}{(H - H_r)^2 + (\Delta H/2)^2}. \quad (1)$$

Here,  $\text{Re} S_{21}$ ,  $S_0$ ,  $H$ ,  $L$ , and  $D$  are the real part of transmission parameter  $S_{21}$ , the offset, the applied magnetic field, and the symmetric and antisymmetric magnitude, respectively [29]. Compared with the single peak of FMR spectrum for Fe/Pd bilayer, the two well-separated peaks appear for Fe/Pd/Fe trilayers, which reveal two resonance modes.

To further verify the dynamic properties of the films, we carried out the in-plane angular dependent FMR measurements. Figure 2(a) shows the measured FMR spectra as a function of the magnetic field azimuth  $\varphi_H$  at the fixed

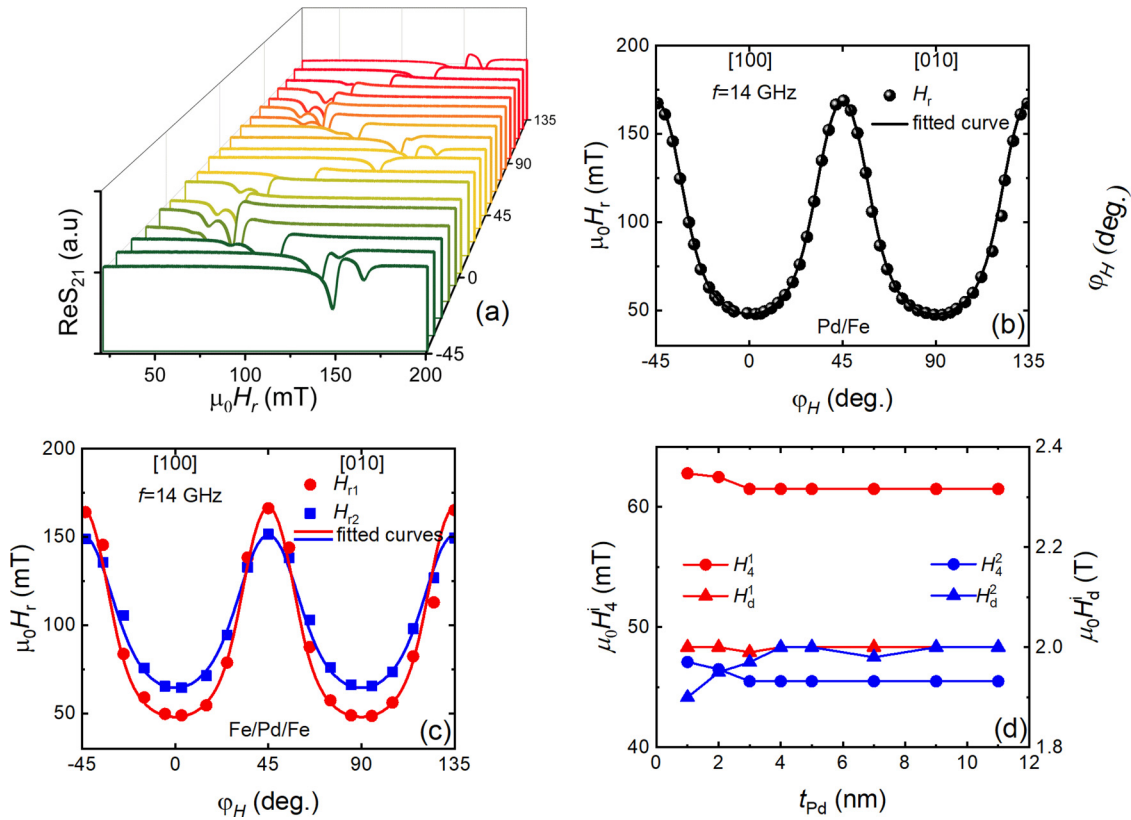


FIG. 2. (a) In-plane angular dependent FMR spectra for Fe(7.5 nm)/Pd(7 nm)/Fe(6 nm) at the fixed frequency 14 GHz. (b) In-plane angular dependence of resonance field  $H_r$  for Pd(7 nm)/Fe(6 nm) bilayers. (c) The extracted resonance field  $H_r$  vs magnetic field angle  $\varphi_H$  from (a). (d) The obtained magnetic anisotropy parameters via fitting the two kinds of the angular relations for Fe(7.5 nm)/Pd( $t_{\text{Pd}}$  nm)/Fe(6 nm) trilayers.

frequency 14 GHz. It is clear that two peaks are well separated at various  $\varphi_H$ . The extracted angular dependent resonance field  $H_r$  is plotted in Fig. 2(c). In comparison with a four-fold angular dependent  $H_r$  curve for Pd(7 nm)/Fe [Fig. 2(b)], two fourfold angular dependent  $H_r$  curves are plotted for Fe(7.5 nm)/Pd(7 nm)/Fe(6 nm) trilayers [Fig. 2(c)], which corresponds to the dispersion relations of the two resonance modes mentioned in Figs. 1(c) and 2(a). The dispersion relation marked by the index  $i, j$  ( $i, j = 1, 2, i \neq j$ ) can be followed via adding the interlayer exchange coupling term into the Kittel formula [32],

$$f^i = \frac{\gamma\mu_0}{2\pi} \sqrt{H_a^i H_b^i}, \quad (2)$$

with  $H_a^i = H_r^i \cos(\varphi_M^i - \varphi_H) + H_d^i + H_4^i(3 + \cos 4\varphi_M^i)/4 + H_{\text{ex}}^i \cos(\varphi_M^i - \varphi_M^j)$  and  $H_b^i = H_r^i \cos(\varphi_M^i - \varphi_H) + H_4^i \cos 4\varphi_M^i + H_{\text{ex}}^i \cos(\varphi_M^i - \varphi_M^j)$ . Here,  $\gamma$ ,  $\mu_0$ ,  $H_4^i$ , and  $\varphi_M^i$  are the gyromagnetic ratio, the vacuum permeability, the fourfold magnetocrystalline anisotropy field, and the azimuthal angle of magnetization in layer  $i$ , respectively.  $H_d^i = M_s^i - \frac{2K_{\text{out}}^i}{\mu_0 M_s^i}$  indicates the effective demagnetizing field with the saturation magnetization  $M_s^i$  and the out-of-plane uniaxial magnetic anisotropy constant  $K_{\text{out}}^i$ .  $H_{\text{ex}}^i = \frac{A_{\text{ex}}}{\mu_0 M_s^i t^i}$  represents the effective interlayer exchange coupling field with the exchange coupling constant  $A_{\text{ex}}$  and the FM layer thickness  $t^i$ . The fitted magnetic anisotropy parameters are plotted in Fig. 2(d). It can be found that  $H_d^2$  has a slight increase, and  $H_4^1$  and  $H_4^2$  decrease slightly when  $t_{\text{Pd}} < \text{nm}$  for the Fe/Pd/Fe trilayers. The effective demagnetizing field  $\mu_0 H_d^1$  for the index 1 of the trilayers and  $\mu_0 H_d$  for Pd/Fe bilayer nearly host the same value of 2 T. Moreover, the value of  $\mu_0 H_4$  is 62.5 mT for Pd/Fe bilayer, which approximates to  $\mu_0 H_4^1$  in the trilayers. Considering the almost identical magnetocrystalline anisotropy field between the index 1 of the trilayers and the bilayers, it is quite understandable to regard the index 1 as the bottom Fe layer of the trilayers. This means that the mode signed by the index 1 is equivalent to the resonant mode of the Pd/Fe bilayers perturbed by an exchange coupling term. Correspondingly, the mode signed by the index 2 represents the excitation of the top Fe layer modulated by the exchange coupling term. Furthermore, the magnetocrystalline anisotropy fields of the two Fe layers are different. It was owing to the difference of lattice mismatch, 3.8% for Fe films grown on the MgO(001) and 5.1% on Pd(001), respectively [33].

The obtained exchange coupling constant  $A_{\text{ex}}$  as a function of the Pd thickness for Fe/Pd/Fe trilayers is plotted in Fig. 4(a). The coupling is ferromagnetic and its strength is decreased when increasing the Pd thickness. The ferromagnetic coupling nearly vanishes in the range of Pd thickness larger than 3 nm. Here, the interlayer exchange coupling is ascribed to the Ruderman-Kittel-Kasuya-Yosida interaction (RKKY) and magnetic dipolar interaction, known as Néel coupling [34]. There are two points to be emphasized. First, as shown in Fig. 4(a), the oscillatory behavior of RKKY with alternating ferromagnetic coupling and antiferromagnetic coupling is suppressed, which is ascribed to the weak induced moment in Pd [33,35]. Second, magnetic dipolar interaction between two Fe layers originates from the morphological corrugation or Pd/Fe interface roughness [29,34,36].

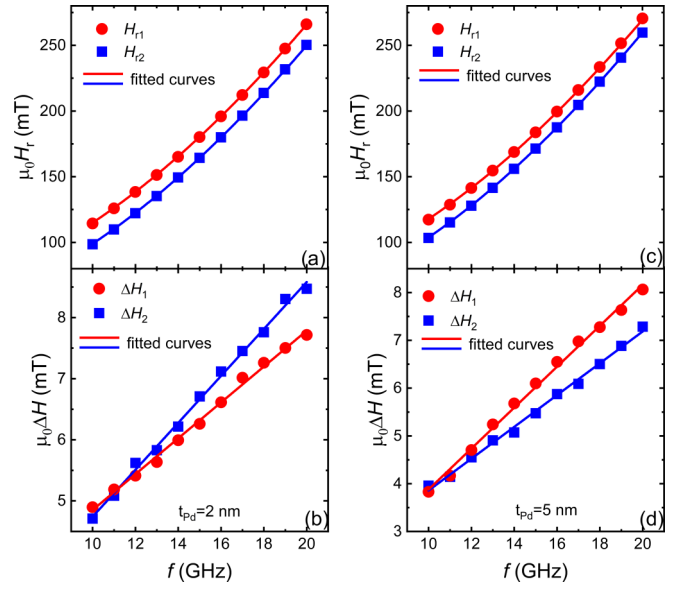


FIG. 3.  $H_r$  vs  $f$  (a) and  $\Delta H$  vs  $f$  (b) for Fe(7.5 nm)/Pd(2 nm)/Fe(6 nm).  $H_r$  vs  $f$  (c) and  $\Delta H$  vs  $f$  (d) for Fe(7.5 nm)/Pd(5 nm)/Fe(6 nm).

Therefore, the 3-nm critical thickness is slightly larger than the reported values ( $\sim 2$  nm) [35].

Figure 3(a) shows the frequency dependence of the resonant field  $H_r$  for the Fe/Pd(2 nm)/Fe trilayers with the applied magnetic field  $H$  along Fe[110]. Two resonance branches are observed. Both branches can be well reproduced by Eq. (2) based on the magnetic anisotropy parameters extracted from Fig. 2(b), thereby signed by the index 1 and 2. The corresponding linewidth scales linearly with the frequency, as shown in Fig. 3(b). The Gilbert damping constant was obtained using the relation

$$\Delta H = \frac{4\pi\alpha f}{\mu_0\gamma} + \Delta H_0, \quad (3)$$

where  $\Delta H_0$  is the inhomogeneous broadening [37]. Similar resonant field and linewidth behaviors are also seen between Fe/Pd(2 nm)/Fe and Fe/Pd(5 nm)/Fe trilayers, as shown in Figs. 3(c) and 3(d). However, it is worth noting that the damping values of the index 1 and 2 in Fig. 3(b) reverse compared with those in Fig. 3(d).

Before discussing the damping of Fe/Pd/Fe trilayers in detail, we first display the Gilbert damping of the bilayers Pd/Fe as a function of Pd thickness, as shown in Fig. 4(b). The damping constants increase with increasing Pd thickness and approach a saturated value, which accords with the spin pumping model. In the spin-pumping model, the magnetization precession results in the nonequilibrium chemical potential imbalance of spin at FM/NM interfaces and thereby leads the angular momentum flow between FM and NM layers, i.e., spin current. With regard to the Pd/Fe bilayers, the heavy metal Pd absorbs the pumped spin current  $\mathbf{j}_s^{\text{pump}}$  via the Elliott-Yafet spin relaxation to enhance the Gilbert damping of Fe films [38]. Partial spin current  $\mathbf{j}_s^{\text{back}}$  flows back to the Fe films to suppress the Gilbert damping via spin transfer torque. As a result, the additional damping depends on the effective spin

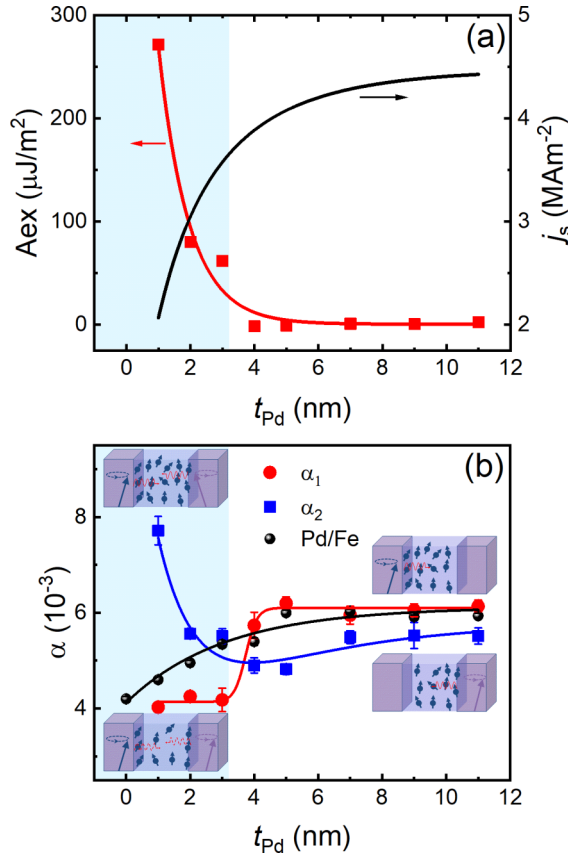


FIG. 4. (a) Interlayer exchange coupling parameter  $A_{\text{ex}}$  vs Pd thickness  $t_{\text{Pd}}$  in Fe/Pd/Fe (red lines and squares). The interlayer exchange coupling region is denoted by color code. Spin current density as a function of Pd thickness (Black line). (b) The Gilbert damping vs Pd thickness for the Pd/Fe bilayers and Fe/Pd/Fe trilayers. Sketches of the magnetization precession represent the different excitation modes. The red line is an eye guide.

current  $j_{\text{eff}}$  [7],

$$j_{\text{eff}} = j_s^{\text{pump}} - j_s^{\text{back}} = \frac{\hbar}{4\pi} g^{\uparrow\downarrow} \mathbf{m} \times \frac{\partial \mathbf{m}}{\partial t}. \quad (4)$$

Here,  $\mathbf{m}$  and  $g^{\uparrow\downarrow}$  are the unit vector of magnetization and effective spin mixing conductance, respectively. In comparison with the short-range interlayer exchange coupling  $\sim 3$  nm in Fe/Pd/Fe, the long-range dynamic coupling signed by spin current density of the Pd layer is calculated using Eq. (4) in the Pd/Fe bilayers, as shown in Fig. 4(a), which indicates the nonequilibrium spin accumulated in a larger scale. In our previous work [29], we have determined the spin diffusion length of Pd  $\sim (6.2 \pm 1.4)$  nm for the Pd/Fe bilayers based on the spin pumping model [29,36]. However, after another Fe layer covers the Pd/Fe bilayers to construct the Fe/Pd/Fe trilayers, a distinct damping tendency is observed. Figure 4(b) summarizes the Pd thickness dependence of the Gilbert damping for the index 1 and 2 of the Fe/Pd/Fe trilayers. It is obviously found that the damping constants of the index 1 and 2 are very different with increasing Pd thickness. When the thickness of Pd is lower than 3 nm, the damping decreases with the increase of Pd thickness for the index 2, while it

keeps unchanged for the index 1. However, in the range of Pd thickness larger than 3 nm, their Gilbert damping constants increase as the thickness of Pd increases. Strikingly, although the resonance mode of the index 1 is in analogy to the Pd/Fe bilayers, it displays a characteristic steplike damping features at  $t_{\text{Pd}} = 3$  nm, where the damping markedly jumps to a saturation value. Meanwhile, the damping of the index 2 decreases to an almost saturation value nearby the 3-nm Pd thickness. Intriguingly, the characteristic length  $t_{\text{Pd}} = 3$  nm matches well with the coupling one in Fig. 4(a).

We first exclude the spurious mechanism behind the observation of Fig. 4(b). The inhomogeneous magnetization distribution from the top Fe layers overlaps the bottom Fe layers to possibly yield a spurious effect on magnetic relaxation. However, the spurious effect just results in the inhomogeneous linewidth broaden [39]. Note that both the resonance linewidth  $\Delta H$  for the index 1 and 2 scale linearly with the resonance frequency  $f$ , as shown in Figs. 3(b) and 3(d), manifesting that the Gilbert damping plays dominant roles rather than the inhomogeneous contribution in magnetic relaxation process. Moreover, even though there is an existing spurious effect, its dominant effect is on the top Fe layers rather than resulting in the steplike damping feature of the index 1.

Our observation can be fully explained by considering the dynamic coupling mediated by the spin pumping-induced spin current in the separated and collective precession modes. The sketches of the precessing magnetizations in Fig. 4(b) represent the underlying relaxation mechanism. We categorize the Pd thickness dependent damping into two regions. First, the static interlayer exchange exits within less than 3-nm Pd thickness, and results in the entanglement of the dynamics of the two Fe layers. That is, there is no separated magnetization precession, in which the precession in one Fe layer drags the magnetization in another Fe layer [40]. Meanwhile, the dynamic coupling mediated by spin current involves in the entanglement of the precession of the two Fe layers according to spin pumping effect. The temporal magnetization  $\mathbf{m}_i$  evolutions are determined by the Landau-Lifshitz-Gilbert (LLG) equation modified by the static interlayer coupling and dynamic coupling [9],

$$\begin{aligned} \frac{\partial \mathbf{m}_i}{\partial t} = & -\gamma \mu_0 \mathbf{m}_i \times (\mathbf{H}_{\text{eff}}^i + J_{\text{ex}} \mathbf{M}_j) + (\alpha_i^0 + \alpha_{ii}^{sp}) \mathbf{m}_i \\ & \times \frac{\partial \mathbf{m}_i}{\partial t} - \alpha_{ij}^{sp} \mathbf{m}_j \times \frac{\partial \mathbf{m}_j}{\partial t}. \end{aligned} \quad (5)$$

Here,  $J_{\text{ex}}$  and  $\mathbf{H}_{\text{eff}}^i$  are the static exchange coupling strength and effective magnetic field, respectively.  $\alpha_i^0$ ,  $\alpha_{ii}^{sp}$ , and  $\alpha_{ij}^{sp}$  are the local damping, the enhanced damping due to the spin current pumped out of layer  $i$ , and the antidamping due to the spin current pumped into layer  $i$  from layer  $j$ , respectively. The eigenmodes of the collective magnetization precession, treated as acousticlike and optical-like modes, can be given via solving the modified LLG equation [41–44]. In a simplified view, magnetization precessions of two coupled Fe layers are mutually triggered into the acousticlike and optical-like modes. In any collective modes, two Fe layers mutually launch spin current. The effective spin current  $j_{\text{eff}}$  is given by

$$j_{\text{eff}} = \sum_i \frac{\hbar}{4\pi} g_i^{\uparrow\downarrow} \mathbf{m}_i \times \frac{\partial \mathbf{m}_i}{\partial t}. \quad (6)$$

Here,  $g_i^{\uparrow\downarrow}$  is the effective spin mixing conductance across the Fe/Pd interface of layer  $i$ . Note that the phase of the launched spin current depends on that of the oscillating magnetization  $\mathbf{m}_i$  [15,45,46]. Considering the spin coherence, the effective spin current is largely enhanced due to the out-of-phase mutual precessions of two Fe layers for acousticlike mode, while it is suppressed due to the in-phase mutual precessions in the acousticlike mode. The index 1 and 2 of the trilayers correspond to the acousticlike and optical-like modes, respectively. Therefore, the additional damping is suppressed in the index 1, while the index 2 shows the giant damping enhancement, as shown in Fig. 4(b). Our experimental results and analysis are supported by the theoretical prediction based on the coherence of spin current [47–49]. Remarkably, the relevant concepts were also proposed in some previous experiments, which also strongly suggest the validity of the mechanism based on the coherent spin current. For example, the oscillation of Gilbert damping of Fe/Au/Pd systems is described by the quantum well state induced spin currents [50]. The phase of spin current can be tuned across NM [51,52].

As shown in Fig. 4(a), the magnitude of interlayer exchange coupling between two Fe layers hinges on the Pd insertion layer thickness. The magnetization precessions are separated when the two Fe layers magnetically decouple by the thicker Pd spacer. The separated precession modes can be described by the following equation:

$$\frac{\partial \mathbf{m}_i}{\partial t} = -\gamma \mu_0 \mathbf{m}_i \times \mathbf{H}_{\text{eff}}^i + (\alpha_i^0 + \alpha_{ii}^{sp}) \mathbf{m}_i \times \frac{\partial \mathbf{m}_i}{\partial t}. \quad (7)$$

In this case, the magnetization precession of one Fe layer is excited by microwave, while another Fe layer is off resonant. The spin current is launched by the precession of Fe layer  $i$ . The effective spin current  $\mathbf{j}_{\text{eff}}$  can be written by

$$\mathbf{j}_{\text{eff}} = \frac{\hbar}{4\pi} g_i^{\uparrow\downarrow} \mathbf{m}_i \times \frac{\partial \mathbf{m}_i}{\partial t}. \quad (8)$$

The pumped spin current is absorbed by the Pd and another Fe layer, which brings about the damping enhancement. The off-resonant Fe layer is a more efficient spin sink with the spin diffusion length of  $\sim 1$  nm compared to Pd [53], resulting in the coherent spin current being dissipated quickly. Therefore, we observe a drastic increase of the damping  $\alpha_{ii}^{sp}$  for the index 1 nearby 3-nm Pd, even though the Pd thickness is thinner

than the spin diffusion length of Pd  $\sim (6.2 \pm 1.4)$  nm. In addition, we also note that the damping of the acoustic (optical) mode monotonously increases (decreases) with increasing the Pt thickness in Py/Pt/Py trilayers in Ref. [23]. Distinct from our study, the damping values of the two modes in Ref. [23] approach equivalence near the static interlayer exchange coupling length  $\sim 3.5$  nm. It is hard to observe a steplike damping tendency in Py/Pt/Py trilayers because the short-range static interlayer exchange coupling length  $\sim 3.5$  nm is even larger than the long-range spin diffusion length of Pt  $\sim 1.1$  nm due to the magnetic proximity effect.

#### IV. CONCLUSION

We have explored the relaxation process of the Fe/Pd/Fe trilayers. In comparison with Pd/Fe bilayers, Pd layer thickness dependence of Gilbert damping indicates a pronounced jump feature at  $\sim 3$  nm, which is the characteristic static interlayer exchange coupling length of Fe/Pd/Fe. The steplike damping feature is ascribed to the entanglement of the two Fe layers mediated by the static exchange coupling and the dynamic exchange coupling. The interlocked magnetization precession by the static coupling leads to the pronounced enhancement or suppression of the Gilbert damping via spin current in trilayers. When the two Fe layers magnetically decouple via inserting thick Pd layer, the pumped spin current from the resonant Fe layer is efficiently absorbed by both the off-resonant Fe layer and the Pd layer, giving rise to the significant enhancement of the nonlocal Gilbert damping. The observation of the anomalous damping features provides insight into manipulating the spin transport and magnetic relaxation through tuning the static interlayer exchange coupling and the dynamic coupling based on the coherence of the spin current.

#### ACKNOWLEDGMENTS

This work was supported by the National Key Research Program of China (Grants No. 2016YFA0300701 and No. 2017YFB0702702), the National Natural Sciences Foundation of China (Grants No. 52031015, No. 1187411, and No. 51871235), and the Key Research Program of Frontier Sciences, CAS (Grants No. QYZDJ-SSW-JSC023, No. KJZD-SW-M01, and No. ZDYZ2012-2).

- 
- [1] Y. Liu, A. A. Starikov, Z. Yuan, and P. J. Kelly, *Phys. Rev. B* **84**, 014412 (2011).
  - [2] L. Chen, S. Mankovsky, S. Wimmer, M. A. W. Schoen, H. S. Körner, M. Kronseder, D. Schuh, D. Bougeard, H. Ebert, D. Weiss, and C. H. Back, *Nat. Phys.* **14**, 490 (2018).
  - [3] B. Khodadadi, A. Rai, A. Sapkota, A. Srivastava, B. Nepal, Y. Lim, D. A. Smith, C. Mewes, S. Budhathoki, A. J. Hauser, M. Gao, J.-F. Li, D. D. Viehland, Z. Jiang, J. J. Heremans, P. V. Balachandran, T. Mewes, and S. Emori, *Phys. Rev. Lett.* **124**, 157201 (2020).
  - [4] V. Kambersky and C. Patton, *Phys. Rev. B* **11**, 2668 (1975).
  - [5] A. Brataas, Y. Tserkovnyak, and G. E. W. Bauer, *Phys. Rev. Lett.* **101**, 037207 (2008).
  - [6] S. Mankovsky, D. Ködderitzsch, G. Woltersdorf, and H. Ebert, *Phys. Rev. B* **87**, 014430 (2013).
  - [7] Y. Tserkovnyak, A. Brataas, and G. E. W. Bauer, *Phys. Rev. Lett.* **88**, 117601 (2002).
  - [8] Y. Tserkovnyak, A. Brataas, G. E. W. Bauer, and B. I. Halperin, *Rev. Mod. Phys.* **77**, 1375 (2005).
  - [9] A. A. Baker, A. I. Figueroa, C. J. Love, S. A. Cavill, T. Hesjedal, and G. van der Laan, *Phys. Rev. Lett.* **116**, 047201 (2016).
  - [10] I. Žutić, J. Fabian, and S. Das Sarma, *Rev. Mod. Phys.* **76**, 323 (2004).
  - [11] I. Razdolski, A. Alekhin, N. Ilin, J. P. Meyburg, V. Roddatis, D. Diesing, U. Bovensiepen, and A. Melnikov, *Nat. Commun.* **8**, 15007 (2017).

- [12] B. Khodadadi, J. B. Mohammadi, J. M. Jones, A. Srivastava, C. Mewes, T. Mewes, and C. Kaiser, *Phys. Rev. Appl.* **8**, 014024 (2017).
- [13] D. A. Arena, E. Vescovo, C. C. Kao, Y. Guan, and W. E. Bailey, *Phys. Rev. B* **74**, 064409 (2006).
- [14] M. Belmeguenai, T. Martin, G. Woltersdorf, M. Maier, and G. Bayreuther, *Phys. Rev. B* **76**, 104414 (2007).
- [15] T. Chiba, G. E. W. Bauer, and S. Takahashi, *Phys. Rev. B* **92**, 054407 (2015).
- [16] M. Li, J. Lu, and W. He, *Phys. Rev. B* **103**, 064429 (2021).
- [17] H. Liu, D. Sun, C. Zhang, M. Groesbeck, R. McLaughlin, and Z. V. Vardeny, *Sci. Adv.* **5**, eaax9144 (2019).
- [18] Y. Li, W. Cao, V. P. Amin, Z. Zhang, J. Gibbons, J. Sklenar, J. Pearson, P. M. Haney, M. D. Stiles, W. E. Bailey, V. Novosad, A. Hoffmann, and W. Zhang, *Phys. Rev. Lett.* **124**, 117202 (2020).
- [19] B. Heinrich, Y. Tserkovnyak, G. Woltersdorf, A. Brataas, R. Urban, and G. E. W. Bauer, *Phys. Rev. Lett.* **90**, 187601 (2003).
- [20] B. G. Park, J. Wunderlich, X. Marti, V. Holy, Y. Kurosaki, M. Yamada, H. Yamamoto, A. Nishide, J. Hayakawa, H. Takahashi, A. B. Shick, and T. Jungwirth, *Nat. Mater.* **10**, 347 (2011).
- [21] S. Klingler, V. Amin, S. Geprägs, K. Ganzhorn, H. Maier-Flaig, M. Althammer, H. Huebl, R. Gross, R. D. McMichael, M. D. Stiles, S. T. B. Goennenwein, and M. Weiler, *Phys. Rev. Lett.* **120**, 127201 (2018).
- [22] A. Kamra, D. M. Polishchuk, V. Korenivski, and A. Brataas, *Phys. Rev. Lett.* **122**, 147201 (2019).
- [23] P. Omelchenko, E. Girt, and B. Heinrich, *Phys. Rev. B* **100**, 144418 (2019).
- [24] Z. Celinski, B. Heinrich, J. F. Cochran, W. B. Muir, A. S. Arrott, and J. Kirschner, *Phys. Rev. Lett.* **65**, 1156 (1990).
- [25] A. F. Franco, C. Gonzalez-Fuentes, J. Åkerman, and C. Garcia, *Phys. Rev. B* **95**, 144417 (2017).
- [26] X. Tao, Q. Liu, B. Miao, R. Yu, Z. Feng, L. Sun, B. You, J. Du, K. Chen, S. Zhang, L. Zhang, Z. Yuan, D. Wu, and H. Ding, *Sci. Adv.* **4**, eaat1670 (2018).
- [27] M. Caminale, A. Ghosh, S. Auffret, U. Ebels, K. Ollefs, F. Wilhelm, A. Rogalev, and W. E. Bailey, *Phys. Rev. B* **94**, 014414 (2016).
- [28] J. M. Shaw, H. T. Nembach, and T. J. Silva, *Phys. Rev. B* **85**, 054412 (2012).
- [29] Y. Li, Y. Li, Q. Liu, Z. K. Xie, E. Vetter, Z. Yuan, W. He, H. L. Liu, D. L. Sun, K. Xia, W. Yu, Y. B. Sun, J. J. Zhao, X. Q. Zhang, and Z. H. Cheng, *New J. Phys.* **21**, 103040 (2019).
- [30] Y. Li, Y. Li, Q. Liu, Z. Yuan, Q.-F. Zhan, W. He, H.-L. Liu, K. Xia, W. Yu, X.-Q. Zhang, and Z.-H. Cheng, *New J. Phys.* **21**, 123001 (2019).
- [31] Y. Li, S.-J. Yang, D. Sun, Y.-B. Sun, Y. Li, E. Vetter, R. Sun, N. Li, X. Yang, L. Su, Z.-Z. Gong, Z.-K. Xie, J.-J. Zhao, W. He, X.-Q. Zhang, and Z.-h. Cheng, *Phys. Rev. B* **102**, 014420 (2020).
- [32] G. B. G. Stenning, L. R. Shelford, S. A. Cavill, F. Hoffmann, M. Haertinger, T. Hesjedal, G. Woltersdorf, G. J. Bowden, S. A. Gregory, C. H. Back, P. A. J. D. Groot, and G. V. D. Laan, *New J. Phys.* **17**, 013019 (2015).
- [33] Z. Celinski, B. Heinrich, and J. F. Cochran, *J. Appl. Phys.* **70**, 5870 (1991).
- [34] J. F. Bobo, L. Gabillet, and M. Bibes, *J. Phys.: Condens. Matter* **16**, S471 (2004).
- [35] D. L. R. Santos, P. Venezuela, R. B. Muniz, and A. T. Costa, *Phys. Rev. B* **88**, 054423 (2013).
- [36] See Supplemental Material at <http://link.aps.org/supplemental/10.1103/PhysRevB.104.094409> for the atomic force microscopy images of bare Fe film and Pd/Fe bilayers and the estimation of the spin diffusion length of Pd.
- [37] R. Urban, G. Woltersdorf, and B. Heinrich, *Phys. Rev. Lett.* **87**, 217204 (2001).
- [38] L. Ma, L. Lang, J. Kim, Z. Yuan, R. Wu, S. Zhou, and X. Qiu, *Phys. Rev. B* **98**, 224424 (2018).
- [39] J. Lindner, K. Lenz, E. Kosubek, K. Baberschke, D. Spoddig, R. Meckenstock, J. Pelzl, Z. Frait, and D. L. Mills, *Phys. Rev. B* **68**, 060102(R) (2003).
- [40] A. A. Timopheev, Y. G. Pogorelov, S. Cardoso, P. P. Freitas, G. N. Kakazei, and N. A. Sobolev, *Phys. Rev. B* **89**, 144410 (2014).
- [41] P. Grünberg and K. Mika, *Phys. Rev. B* **27**, 2955 (1983).
- [42] A. Layadi, *Phys. Rev. B* **65**, 104422 (2002).
- [43] J. Lindner and K. Baberschke, *J. Phys.: Condens. Matter* **15**, S465 (2003).
- [44] Y. Wei, S. Jana, R. Brucas, Y. Pogoryelov, M. Ranjbar, R. K. Dumas, P. Warnicke, J. Åkerman, D. A. Arena, O. Karis, and P. Svedlindh, *J. Appl. Phys.* **115**, 17D129 (2014).
- [45] T. Taniguchi, *Phys. Rev. B* **97**, 184408 (2018).
- [46] T. Taniguchi, *Phys. Rev. B* **98**, 104417 (2018).
- [47] Y. Tserkovnyak, A. Brataas, and G. E. W. Bauer, *Phys. Rev. B* **67**, 140404(R) (2003).
- [48] H. J. Jiao and G. E. W. Bauer, *Phys. Rev. Lett.* **110**, 217602 (2013).
- [49] S. Takahashi, *Appl. Phys. Lett.* **104**, 052407 (2014).
- [50] E. Montoya, B. Heinrich, and E. Girt, *Phys. Rev. Lett.* **113**, 136601 (2014).
- [51] J. Li, L. R. Shelford, P. Shafer, A. Tan, J. X. Deng, P. S. Keatley, C. Hwang, E. Arenholz, G. van der Laan, R. J. Hicken, and Z. Q. Qiu, *Phys. Rev. Lett.* **117**, 076602 (2016).
- [52] Q. Li, M. Yang, C. Klewe, P. Shafer, A. T. N'Diaye, D. Hou, T. Y. Wang, N. Gao, E. Saitoh, C. Hwang, R. J. Hicken, J. Li, E. Arenholz, and Z. Q. Qiu, *Nat. Commun.* **10**, 5265 (2019).
- [53] A. Ghosh, S. Auffret, U. Ebels, and W. E. Bailey, *Phys. Rev. Lett.* **109**, 127202 (2012).